Radar Range-Breathing Separation for the Automatic Detection of Humans in Cluttered Environments

Emanuele Cardillo, Member, IEEE, and Alina Caddemi, Member, IEEE

***Abstract*—In this paper, a new sensing approach for the automatic detection and ranging of human targets in cluttered environments is detailed. The person detection does not require to preliminarily define a target threshold, thus minimizing the likelihood of false alarm events. Moreover, the proposed approach allows to resolve the artifacts due to the presence of multiple objects within the same radiation beam without increasing the system complexity and cost. A powerful graphical representation, denominated range-breathing graph, is exploited for quickly making the reader aware of the exact human location, employing the breathing rate as the key element for discerning between humans and non-human targets. The method is analytically described while exhaustive simulations are carried out for confirming the reliability and suitability of the method with regard to the state of art. The effectiveness of the range-breathing separation approach is demonstrated by using two different radar boards operating at the frequencies of 24 GHz and 122 GHz. The obtained results show the general validity of this approach for identifying humans in complex cluttered scenarios**

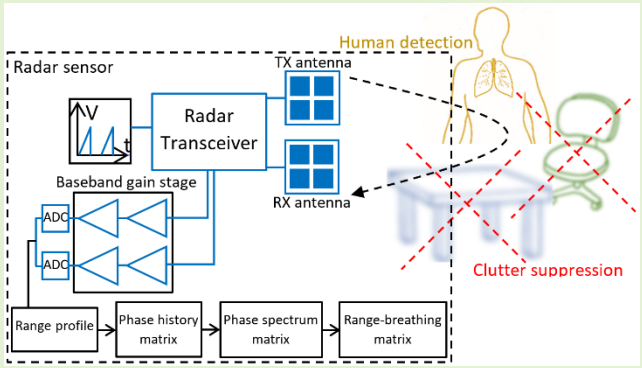

***Index Terms*— Vital signs, breathing rate measurement, microwave radar, FMCW waveform, human target detection, short-range radars, contactless sensors.**

I. Introduction

THE task of detecting and locating humans in both indoor and outdoor environments is gaining strong interest for civil, medical, industrial and military applications [1] - [5].

The main examples include but are not limited to the capability of detecting buried people under debris, positioning and navigation, intrusion detection or health-care surveillance.

The human detection often relies on contact-based transducers, infrared sensors or optical/vision systems [6] - [11]. While worn contact-based transducers might compromise the user's comfort, infrared sensors are very sensitive to different ambient light and temperature conditions. Although the optical/vision systems might provide precise localization of human targets upon normal operations, different ambient light conditions seriously limit their performance [12] - [13]. The related privacy concerns make this technology unsuitable for a wide set of applications. Moreover, camera-based systems could be considered bulky if compared to the dimensions of the circuits operating at very high frequencies, i.e. millimeter-waves.

In this framework, the microwave and millimeter-wave radar technology is showing a disruptive impact in terms of reliability, precision and multiplicity of provided information for short-range applications [14] - [18]. Moreover, radar sensors can be considered un-intrusive systems that simultaneously preserve the privacy of the users. Avoiding privacy concerns is not only a matter of improving the users' comfort but rather it is a serious topic involving restrictive regulations and limitations to the usability and applicability of the available systems, especially in smart environment [19] - [21]. The task of detecting the human presence in short-range environments usually relies on the detection of vital signs, e.g. the breathing rate [22] - [25]. To this purpose, the unmodulated continuous wave (CW) and the frequency modulated continuous wave (FMCW) are the two most employed radar techniques [25]. The main advantage of CW over FMCW concerns the better precision in measuring speeds and displacements, thus allowing to measure sub-millimeter range shifts [15] - [16]. Nevertheless, it lacks in the ability of measuring absolute ranges, which instead is one of the main features of FMCW radars [12]. Despite the great strides made by the research, the wide number of recent scientific articles proves that the human detection is still a challenging task and the existing solutions are not fully suitable to be completely automated. In [27], a valuable solution involving the scene reconstruction through 2 D radar imaging has been proposed. A 5.8 GHz radar mounted on a tripod for achieving a mechanical rotation has

Emanuele Cardillo and Alina Caddemi are with the Department of Engineering, University of Messina, 98100, Messina, Italy (e-mail: ecardillo@unime.it; acaddemi@unime.it).

been employed to identify a human target by exploiting both FMCW and interferometry modes and analyzing different echo signals from different angles-of-arrivals. In [28], a self-injection-locked radar system on a mobile platform has been used for detecting and monitoring the position of concealed humans in a 2-D image. Besides requiring the radar motion for scanning the scenario, this system must be maintained in every scanning position for a long time. In [29], a moving platform has been employed for measuring the breathing rate of human targets, meanwhile removing the radar motion effects by means of a reference signal derived from an RF tag worn by the person. In [30], a fundamental and harmonic dual-frequency radar detected the human vital sign eliminating the radar motion effects. However, the system required a stationary reflector, whereas the radar was vibrating rather than exactly moving. In [31], [32], mobile radar systems whose movement is accomplished by employing a drone and a sliding platform, respectively, generated a 2-D target image for identifying human targets. In [33], Multiple-Input-Multiple-Output (MIMO) architectures have been employed for coherently combining the same signal with different phases, thus greatly improving the target sensing. In [34], multiple human targets have been detected and tracked by using a multi-receiver radar board, exploiting an angle estimation algorithm to ensure high robustness against false alarm and ghost targets. In [35], Doppler processing and spectral estimation are concurrently exploited for detecting the vital signs of multiple targets located at distances shorter than the radar spatial resolution, eliminating the mutual interference by means of a range integration algorithm. In [36], a mm-wave radar has been employed for the remote monitoring of human signs. Although it shows relevant results, both a preliminary target recognition step and computationally onerous algorithms are required. Even though for a different application, a range-vibration map has been proposed in [37] to search for the best range bin that minimizes the vital sign estimations errors. However, this method has been selectively applied to small sub-range of the surrounding space, thus not accounting for the interaction between different targets. Therefore, it might not be used for the human detection in its current form. The above-mentioned solutions require to place the radar on a moving platform or to employ complex radar architectures and signal processing techniques for dealing with the noise arising from the artifacts due to the presence of multiple objects. Although these solutions are attractive for their capability to effectively solve this issue, this task has been performed at expenses of system complexity and cost.

A novel feature introduced in this paper concerns the ability of detecting multiple humans against clutter within the same antenna radiation beam, thus avoiding the increased system complexity and cost required by the existent techniques. The task of establishing whether a target is human or not usually depends on the detection of a vital sign like the breathing, whereas the echo is considered a target of interest upon it passes a threshold defined through a target detection algorithm [38]. Therefore, a not properly selected threshold could involve missing targets or false alarms, thus affecting the system reliability. A further element of novelty in this paper consists of the capability to determine the position of all the humans within the operating scenario without employing a threshold, as an inherent consequence of the adopted technique. Moreover, the achieved results are provided by exploiting a graphical representation denominated range-breathing graph that allows a quick detection and ranging of the human targets. Even though with different goals and methodology, the range-breathing graph is inspired by the well-known range-Doppler algorithm. As the latter allows to quickly discern whether the target is stationary or not, in a similar fashion, the range-breathing separation graph allows to straightforwardly recognize and locate breathing targets in a complex environment, at a glance.

To the authors' best knowledge, this is the first contribution where the human's recognition is automated within the same radiation beam and where the results are provided with such an intuitive and powerful representation.

The paper is organized as follows. In Section II, a comprehensive theoretical description of the method and the proposed procedure are reported. The analytical steps are supported by the simulation of the scenario. In Section III, the effectiveness of the theoretical analysis is experimentally demonstrated and the main results are illustrated by employing two different radar boards operating at the central frequencies of 24.15 GHz and 122.5 GHz. Finally, the conclusions are drawn in Section IV.

II. RANGE-BREATHING SEPARATION THEORY

The range-breathing approach exploits the detection of the breathing signal as a signature for separating human from non-human targets. To this aim, an automated detection procedure has been implemented and hereafter described by assuming to employ an FMCW radar sensor.

A. Theoretical Background

In conventional FMCW radars, the frequency-modulated signal is generated by a voltage-controlled oscillator (VCO) and, after passing through an amplification stage, transmitted by means of the antenna. The linear modulating signal used in this paper is saw-tooth shaped. The mathematical expression for the transmitted electromagnetic signal $s_{tx}(t)$ can be formulated as [39]

$$s_{tx}(t) = e^{j\left(2\pi f_c t + \pi \frac{B}{\tau} t^2 + \phi_0\right)} \quad (1)$$

where f_c is the center frequency, B is the bandwidth of the modulated chirp, τ is the duration time of a single saw-tooth ramp and ϕ_0 is the initial phase. When a human is located within the radiation beam of the antenna, the transmitted signal is back-reflected towards the radar. After the antenna reception and the low-noise amplification, if the signal-to-noise ratio of the received signal $s_{rx}(t)$, is adequate to be detected, it can be expressed as [40]

$$s_{rx}(t) = \sigma\, e^{j\left(2\pi f_c (t-\Delta t) + \pi \frac{B}{\tau}(t-\Delta t)^2 + \phi_0\right)} \quad (2)$$

where σ is the amplitude of the received signal and Δt is the round-trip time

$$\Delta t = \frac{2(R+x(t))}{c} \tag{3}$$

where c is the speed of the light, R is the range of the object and $x(t)$ is the time-varying tiny displacement of the human chest due to the breathing activity. As a matter of fact, this analysis ignores the possible additional random movements of the body that however might be removed during the post-processing steps [41]. After passing through an In-phase and Quadrature (IQ) demodulator and a low-pass filtering stage, the beat signal $s_b(t)$ becomes

$$s_b(t) = \sigma\, e^{j\left(2\pi \frac{B}{\tau}\Delta t\, t + 2\pi f_c \Delta t + \phi_1\right)} \tag{4}$$

where

$$\phi_1 = \pi \frac{B}{\tau} \Delta t^2 \tag{5}$$

is the residual phase component that might be neglected for short-range applications, namely when $\Delta t^2 \ll t\Delta t$ [41]. The first term in the exponent of (4) is attributed to the sinusoidal beat signal generated by the back-scattered echo. During a single chirp, the time shift due to the chest displacement $x(t)$ is very small and the object might be considered stationary in the fast-time space. This involves that the beat frequency f_b might be considered directly related to the range of the object by means of

$$f_b = \frac{2\frac{B}{\tau}\mathrm{R}}{c} \tag{6}$$

The second term in the exponent of (4) analyzed through multiple chirps, represents the slow-time phase history. It is exploited for extracting the chest displacement as

$$x_{[n,m]} = \frac{\varphi_{[n,m]}}{4\pi f_c} c \tag{7}$$

where $x_{[n,m]}$ is the chest displacement due to the breathing physiological motion that in turns modulates the phase $\varphi_{[n,m]}$ computed at the mth bin in the slow-time, within the nth range bin in the fast-time. The notation has been moved from a continuous-time notation to a discrete-time notation because the beat signals are usually acquired and digitally converted in a set of bins $[n,m]$ ($n = 1, 2, \dots, N$ and $m = 1, 2, \dots, M$), where N is the number of samples-per-chirp (fast-time) and M is the number of transmitted chirps (slow-time). The extraction of the phase history works out correctly only if the object remains in the same position, i.e. in the same nth range-bin, during all the phase history processing. Otherwise, a range-alignment algorithm must be implemented before evaluating the phase [43]. The phase is limited within the interval $(-\pi, \pi)$, thus the phase difference between two consecutive chirps must not exceed the boundary of 2π for avoiding phase ambiguities. Moreover, in practical applications, a phase un-wrapping algorithm could be required for extending the phase history values beyond these boundaries [44].

B. Automated Range-Breathing Separation

The radar system has been simulated by employing a transmitted bandwidth sweeping from 122 GHz to 123 GHz, i.e. 1 GHz bandwidth centered at 122.5 GHz, to provide the range resolution of 15 cm. The duration time of a single saw-tooth ramp and the time between successive chirps have been set equal to 350 μs and 74 ms, respectively. These two parameters must be chosen to guarantee a phase difference between two consecutive chirps not exceeding 2π, for the reason described in Section II A. In Fig. 1, the transmitted waveform and the main parameters have been shown. The initial step of the algorithm consists of (a) performing a DC offset compensation, (b) implementing a fast Fourier transform (FFT) over each chirp along the fast time and then (c) computing the range R from (6). The typical outcome is the range profile graphically represented in Fig. 2. A Blackman window (window length equal to the number of samples-per-chirp) has been applied prior to implement the range FFT. In detail, it shows the range profile of two people and a stationary non-human target at the distance of 2 m, 3 m, and 5 m from the radar, respectively. Note that even though the simulated environment might be considered quite complex due to the presence of multiple human and non-human targets within the same antenna radiation beam, it does not circumvent the important issues arising from the so-called random body movement [45], which remain a significant task still to be accomplished as further research work. Typical values have been chosen as vital parameters for the two human targets, i.e. breathing frequency and amplitude, simulating a scenario as close as possible to a real one. The two breathing rates are 12 bpm and 20 bpm, whereas the breathing amplitudes are ± 2.5 mm and ± 3.5 mm for the person at 2 m and 3 m, respectively. The corresponding maximum range shift between two consecutive chirps is 0.23 mm and 0.54 mm, respectively, thus complying with a phase difference not exceeding 2π. The next step that is usually performed consists of extracting the phase history only for the range bins showing the targets' presence [43]. The outcome of this step is the phase history $\varphi(t)$ from which the displacement $x(t)$ can be straightforwardly extracted by means of (7). In Fig. 3, the chest displacements of the two human targets are shown before and after the unwrapping procedure. This widely adopted method is based on a correct detection of every target. However, if a target is lost, e.g. because of a high clutter level or a bad threshold selection, the corresponding chest movement will not be measured and the human target will not be identified.

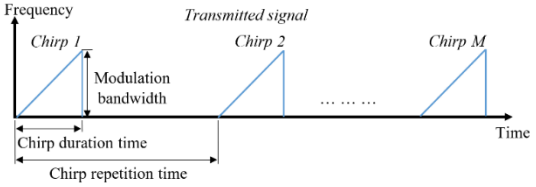

Fig. 1. Transmitted waveform and main parameters.

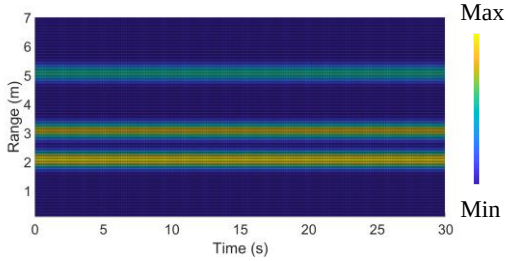

Fig. 2. Simulated range profile of two people and a stationary non-human target at the distance of 2 m, 3 m, and 5 m from the radar, respectively.

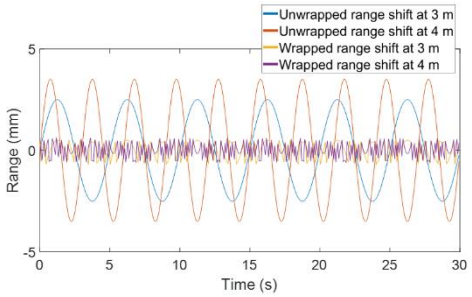

Fig. 3. Simulated chest displacement of the two human targets before and after the unwrapping procedure.

The proposed procedure is aimed at overcoming this limitation, thus pointing towards a reliable and automated detection of each human target within the environment. The second step of the method consists in extracting and unwrapping the phase for each range bin. The resulting data are organized in a matrix, i.e. the phase history matrix, where the columns are the phase histories and the rows are the range bins. Since the phase extraction might be based on relatively simple algorithms, e.g. the arctangent demodulation, this might not excessively burden the computational cost of the algorithm, temporarily solving the problem. The term "temporarily" has been used because the problem is only shifted to the next step. Now, the task is detecting the possible presence of vital signs within all range bins. There are three different possibilities:

1. There are no movements.
2. There are movements whose amplitude and period are compatible with those of the vital signs.
3. There are movements not compatible with those of the vital signs. These movements, e.g. a window opened by the wind or a moving car, could be easily classified and removed.

The third step of the proposed technique consists in performing an additional FFT over the extracted phase history. If one or more breathing targets are detected, the spectrum computed over the phases, $S_\varphi(f)$, will exhibit one or more peaks centered at the breathing frequencies F_{breath}. The resulting data are again arranged in a matrix where the phase history columns of the previous step are now replaced by the corresponding frequency spectrum, i.e. the phase spectrum matrix. The last step consists of multiplying the phase spectrum matrix by the range profile matrix thus resulting in the range-breathing matrix. The magnitude of the range profile data computed in the first step, after the multiplication step, is reduced upon moving away from F_{breath} whereas it is increased upon approaching F_{breath}. Four different cases could arise:

1. One or more breathing targets are present at a certain range bin. Consequently, $S_\varphi(f)$ exhibits strong peaks centered at F_{breath} that multiplied by the corresponding range profile will enhance the signal strength, because the human echo is multiplied by the peak value of $S_\varphi(f)$.
2. One or more non-breathing stationary targets are present at a certain range bin. $S_\varphi(f)$ does not exhibit peaks thus the multiplication by the corresponding range profile in turns will decrease the signal strength.
3. No targets are present at a certain range bin. $S_\varphi(f)$ shows no peaks or complex frequency components due to spectrum leakage, whose effect is eliminated by the magnitude of the corresponding range profile that has a low level due to the absence of a target echo.
4. One or more non-breathing targets exhibiting vibrating or periodical motions, e.g. a fan, window blinds in front of an open window, are present within the range profile. If their frequencies fall out of the respiration interval, they can be easily filtered out. Otherwise, their removal might become challenging since they appear as breathing objects. This last issue is currently object of study within the available scientific literature and might require additional signal processing steps.

It is worth noting that the multiplication step is required to enhance the signal-to-noise ratio of the phase components coming from the human targets. Indeed, the range bins with no targets can be characterized by residual phase components, e.g. due to spectrum leakage, making the phase spectrum complex and the human detection challenging. The multiplication by the range profile allows to rule out the undesired components thus excluding the range bins with no targets. On the other hand, this step enhances the capability of detecting weak echoes coming from human targets, because their low magnitude is multiplied by the peak value of the additional FFT over the phases. This peak amplitude does not depend on the echoes magnitude but rather from the amplitude of the physiological chest displacement that is definitively more pronounced than the zero motion of non-breathing targets. A matrix representation of the processing steps is shown in Fig. 4. In the range profile matrix, two targets are represented: a breathing and a stationary object in rows 2 and 4, respectively. An FFT has been computed on the phase histories for each range bin. In the resulting phase spectrum matrix, the stationary target row has been filled with zeros involving the absence of phase shifts. On the other hand, row 2 shows a one centered at the breathing frequency peak. Residual phase components could occur in range bins with no targets: this event has been considered by adding a one in row 1. Eventually, the multiplication of the phase spectrum matrix by the range breathing matrix will highlight the target presence, automatically deleting both stationary targets and undesired residual phase components.

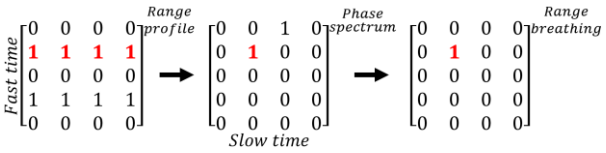

Fig. 4. Matrix signal processing steps.

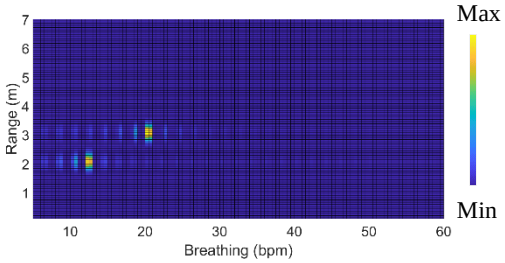

Fig. 5. Range-breathing graph for simulated scenario.

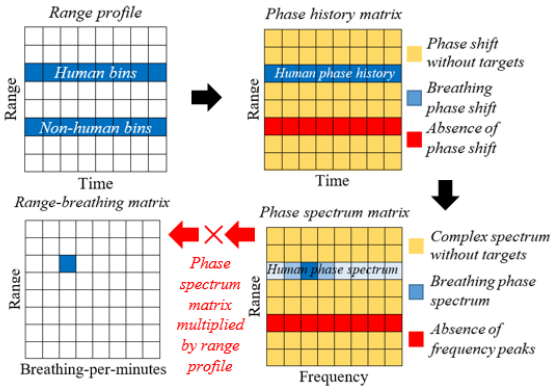

Fig. 6. Flow diagram of the range-breathing method.

TABLE I
SIGNAL PROCESSING STEPS

Step number	Performed task	Task's outcome
1	FFT along the fast time	Range profile
2	Extraction of the phase history for each range bin	Phase history matrix
3	FFT along the phase history matrix	Phase spectrum matrix
4	Multiplication between the phase spectrum matrix and the range profile matrix	Range-breathing matrix
5	Graphical representation	Range-Doppler graph

Moreover, the outcome of the last step, where the breathing frequencies are converted to breathing-per-minutes (bpm), i.e. the range-breathing matrix, is graphically represented by introducing a new graph type inspired by the well-known range-Doppler graph, here referred to as range-breathing graph. As the range-Doppler graph allows to quickly discern whether a target is stationary or not, in a similar fashion, the range-breathing graph is a three-dimensional surface plot, that allows identifying all the breathing targets and their location, at a glance. The x-, and y- axes represent the breathing rate and the range, respectively, whereas the color varies according to the magnitude. The range-breathing graph concerning the simulated scenario is shown in Fig. 5. It is worth noting that not only the stationary target has been totally removed but moreover this task has been automatically accomplished without the need for a threshold-based algorithm aimed at the target detection. The signal processing steps, the performed tasks and their outcome are summarized in Table I, whereas the flow diagram of the range-breathing method is illustrated in Fig. 6. In Section III, the procedure has been applied to different real cases, highlighting its main features and reliability. It is interesting to compare the range-breathing to the range-Doppler method for highlighting the key differences. The range-Doppler processing, after the fast-time FFT aimed at computing the range profile, requires a slow-time FFT along the range profile for obtaining the Doppler components of the targets. The range-Doppler processing applied to the case-of-studies of the present contribution might show the Doppler components of the human breathing. Unfortunately, this is not a sufficient feature for properly distinguishing between human and not human targets. Indeed, since additional not human but moving objects could be present within the environment, their Doppler components could be confused with those of the human, thus making the human separation very challenging. In the range-breathing processing the second FFT is computed on the phase history matrix, thereafter the obtained phase spectrum matrix will be multiplied by the range profile matrix. These two steps are the keys for obtaining the range-breathing map thus providing an intuitive representation of the humans at the different ranges, automatically excluding not-breathing targets.

III. EXPERIMENTAL RESULTS

The effectiveness and the general validity of the procedure have been demonstrated by employing two radar boards, operating within the 24 GHz and 122 GHz Industrial, Scientific and Medical (ISM) bands. Two different radar boards have been used with the aim of testing the effectiveness and the reliability of the proposed approach for different case-of-studies. The 24 GHz radar board exploits an Infineon BGT24MTR11 SiGe transceiver chipset [46]. It is also equipped with both transmitting and receiving antennas and a microcontroller for driving the transceiver and sending the row *IQ* data to the computer through an UART interface. The duration time of a single saw-tooth ramp, the bandwidth and the chirp repetition time have been set equal to 2 ms, 200 MHz (24.05 GHz-24.25 GHz) and 9 ms, respectively. The radar parameters have been chosen for providing suitable maximum measurable phase shifts and ranges, whereas the spatial resolution of 75 cm resulting from the 200 MHz bandwidth is the maximum allowed value within the 24 GHz ISM band [12]. The 122 GHz board employs a Silicon Radar TRX_120_002 on-chip frontend, including a SG13S SiGe BiCMOS transceiver circuit with on-chip antennas [47]. The board also employs a microcontroller whose main tasks are driving the transceiver and providing the communications with the computer. The duration time of a single saw-tooth ramp has been set equal to 350 μs, the bandwidth equal to 1 GHz (122 GHz-123 GHz), whereas the chirp repetition time equal to 74 ms, as the radar platform simulated in Section II. In both cases, the received raw data are sent to the computer for processing. A picture of the experimental set-up has been shown in Fig. 7, where different cluttered configurations have been tested.

A. 24 GHz radar sensor

The first measurement illustrates how the procedure can be exploited for detecting the presence of a human target when multiple targets are concurrently present. In detail, a person at the distance of 4 m from the radar is going to be identified in presence of a metallic target and a wall at the distance of 2.3 m and 6.5 m, respectively. Fig. 8a highlights that the target echo at 4 m is almost undiscernible due to the presence of the strong echoes originated from the two stationary targets. In Fig. 8b, the outcome of the proposed procedure has been shown by means of the range-breathing graph. Unlike the solutions illustrated in [27]-[35], the task of identifying the human target has been accomplished with a reduced system complexity, in a cost-effective way.

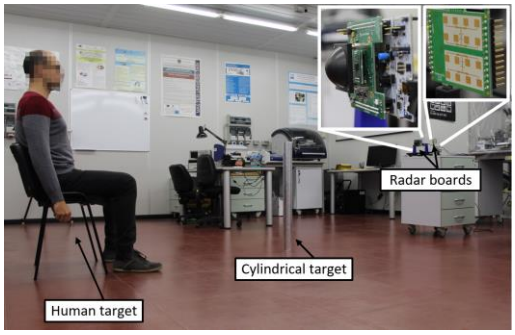

Fig. 7. Picture of the experimental set-up with the inset of the (right) 24 GHz and (left) 122 GHz radar boards.

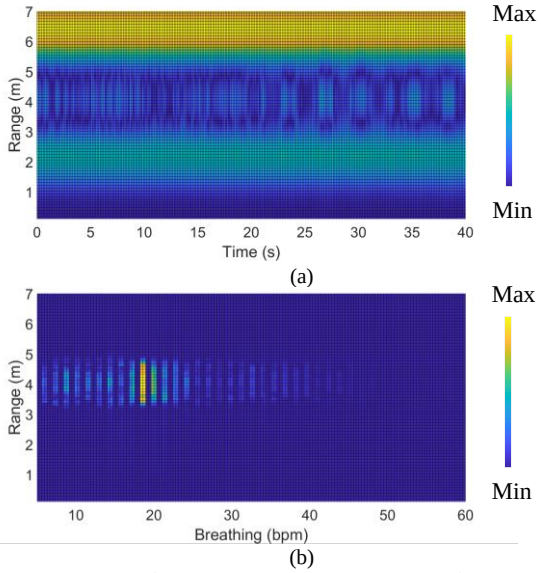

Fig. 8. (a) Range profile and (b) range-breathing graph of a non-human target, a person and a wall at the distance of 2.3 m, 4 m and 6.5 m, respectively. $f_c = 24.15\ GHz$.

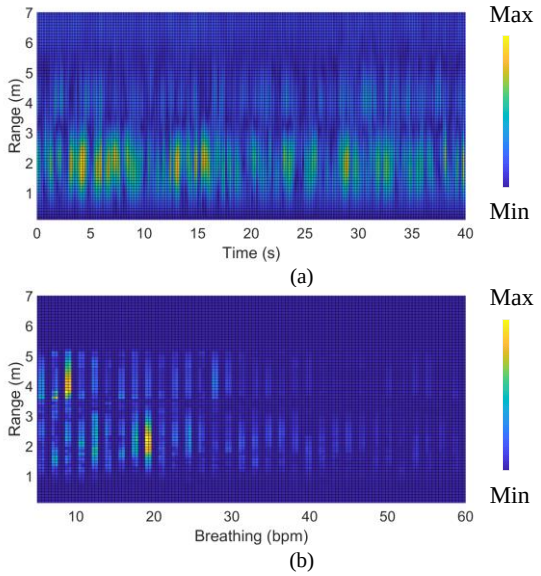

Fig. 9. (a) Range profile and (b) range-breathing graph of two people at the distance of 2 m and 4 m and a desk at the distance of 6 m. $f_c = 24.15\ GHz$.

Unlike the solution proposed in [35], the multiplication between the phase spectrum and the range profile matrix step adds the feature of detecting weak echoes also in complex environments. During the measurement, the respiratory frequency of the subject under test has been monitored by manually counting the chest displacements per unit time obtaining the values of 19 bpm that is in good agreement with the reported result. Thereafter, the procedure has been applied for the complex task of detecting the concurrent presence of two people within the same antenna radiation beam. The tested scenario is composed by two people located at the distance of 2 m and 4 m and a desk at the distance of 6 m. As shown in Fig. 9b, the range-breathing process applied on these data highlights the presence of the two people. The obtained results are in good agreement with the manually measured values of 10 bpm and 20 bpm for the person at 2 m and 4 m, respectively. They can be compared to the range-vibration map performance of [36]. Whereas in this work the vital sign detection of multiple subjects has been demonstrated in a relatively wide scenario, the system proposed in [36] has been exploited for monitoring a subject in the very short-range of 50 cm, i.e. the distance from the radar to a bedroom, with a high sensitivity to micron displacements.

B. 122 GHz radar sensor

Finally, the procedure has been tested with the 122 GHz radar board. In Fig. 10a, a metallic target, a person and a wall are located at 1 m, 2.5 m and 6 m from the radar, respectively. The human figure is partially covered by the metallic target, thus resulting in a weak echo. This cluttered environment has been set with the purpose of testing the method in complex scenarios. Fig. 10b illustrates that the human identification is feasible even with strong additional echoes within the scene. Indeed, the high levels of the echoes coming from the metallic target and the wall are multiplied by the phase spectrum that is close to zero at those range bins. Conversely, the weak human echo is multiplied by the strong phase spectrum peak centered at his breathing rate, enhancing his magnitude and thus allowing to properly identify the presence of the person. This result is in good agreement with the manually measured values of 15 bpm.

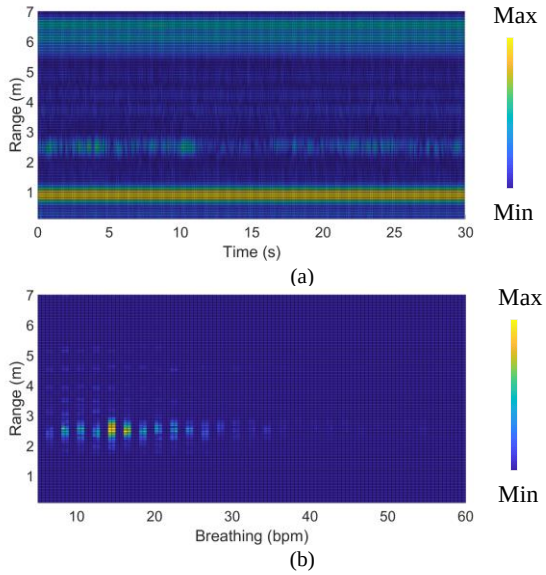

Fig. 10. (a) Range profile and (b) range-breathing graph of a metallic target, a person and a wall located at 1 m, 2.5 m and 6 m from the radar, respectively. $f_c = 122.5\ GHz$.

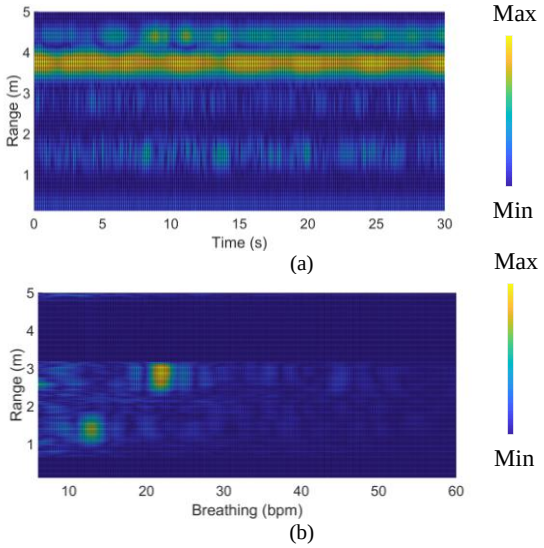

Fig. 11. (a) Range profile and (b) range-breathing graph of two people at the distance of 1.5 m and 2.9 m and a desk at the distance of 6 m. $f_c = 122.5\ GHz$.

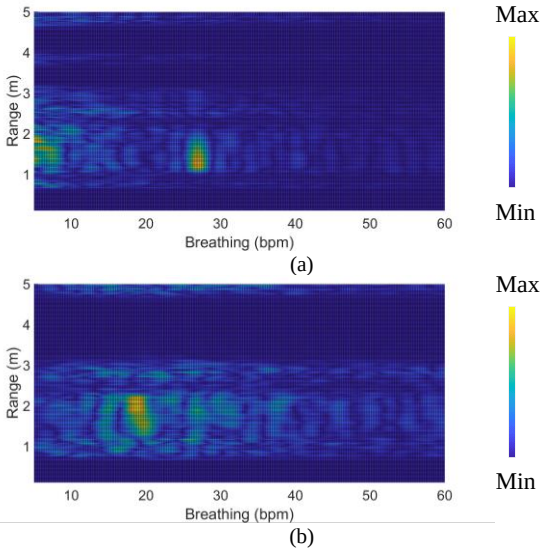

Fig. 12. Range-breathing graph of two people at the same distance. The measurement is not repeatable. $f_c = 122.5\ GHz$.

As for the 24 GHz radar, the concurrent detection of two people at the distances of 1.5 m and 2.9 m has been demonstrated in Fig. 11, by employing the 122 GHz radar board. On the other hand, if two people are located at the same range bin, the mutual interferences between the echoes make the measurements more complex and barely replicable. Two measurements have been shown in Fig. 12 at the same conditions, i.e. two people at 1.5 m whose breathing rates are 20 bpm and 30 bpm. Nonetheless, since the first measurement showed the breathing rate of 20 bpm, whereas the second one highlighted the value of 30 bpm, the concurrent people detection was not accomplished. This might be due to the presence of a predominant echo that alternately highlights the vital signs of one person rather than another one, making the people separation at the same range a challenging task.

IV. Conclusion

This work presents a new method for the automatic detection of human targets by exploiting the features of radar sensors. The method does not require any preliminary target detection step, moving platform or MIMO architecture, thus accomplishing the task with a limited system complexity and cost. The human recognition is automatically fulfilled within the same radiation beam and the results are provided with an intuitive and powerful representation. After analytically describing the procedure, the effectiveness of the approach has been proven by simulating the operating scenario. Finally, two different radar boards operating at microwave and millimeter-wave frequencies have been employed, thus evidencing the general validity of the procedure.

References

[1] S. Yu and T. Horng, "Highly linear phase-canceling self-injection-locked ultrasonic radar for non-contact monitoring of respiration and heartbeat," *IEEE Trans. Biomed. Circ. Syst.*, vol. 14, no. 1, pp. 75-90, Feb. 2020.

[2] K. Peng and J. Lee, "A novel active/passive dual-mode sensing technique for detecting vital signs," *IEEE Trans. Microw. Theory Techn.*, vol. 68, no. 1, pp. 414-424, Jan. 2020.

[3] Y. He, C. Gu, H. Ma, J. Zhu and G. V. Eleftheriades, "Miniaturized circularly polarized Doppler radar for human vital sign detection," *IEEE Trans. Antennas Propag.*, vol. 67, no. 11, pp. 7022-7030, Nov. 2019.

[4] D. Zankl, S. Schuster, R. Feger and A. Stelzer, "What a blast!: a massive MIMO radar system for monitoring the surface in steel industry blast furnaces," in IEEE Microw. Mag., vol. 18, no. 6, pp. 52-69, Oct. 2017

[5] E. Cardillo, and A. Caddemi, "A review on biomedical MIMO radars for vital sign detection and human localization," Electronics, vol. 9, no. 9, 1497, Sept. 2020.

[6] J.Han, L. Shao, D. Xu, and J. Shotton, "Enhanced computer vision with Microsoft kinect sensor: A review," *IEEE Trans. Cybern.*, vol. 43, no. 5, pp. 1318–1334, Oct. 2013.

[7] J. A. Ward, P. Lukowicz, G. Troster, and T. E. Starner, "Activity recognition of assembly tasks using body-worn microphones and accelerometers," *IEEE Trans. Pattern Anal. Mach. Intell.*, vol. 28, no. 10, pp. 1553–1567, Oct. 2006.

[8] T. P. Van Nguyen, L. Tang, F. Hasan, N, D, Minh, and S. Mukhopadhyay "Nature-inspired sensor system for vital signs detection," *Sensor Actuat A-Phys*, vol. 281, no.1, pp. 76-83, Oct. 2018.

[9] E. Cippitelli, F. Fioranelli, E. Gambi, and S. Spinsante, "Radar and RGB-depth sensors for fall detection: A review," *IEEE Sensors J.*, vol. 17, no. 12, pp. 3585–3604, Jun. 2017.

[10] H. Chang et al., "A Method for respiration rate detection in wrist PPG signal using Holo-Hilbert spectrum," *IEEE Sens. J.*, vol. 18, no. 18, pp. 7560-7569, 15 Sept.15, 2018.

[11] O. D. Lara and M. A. Labrador, "A survey on human activity recognition using wearable sensors," *IEEE Commun. Surveys Tuts.*, vol. 15, no. 3, pp. 1192–1209, Jul. 2013.

[12] E. Cardillo, V. Di Mattia, G. Manfredi, P. Russo, A. De Leo, A. Caddemi, and G. Cerri, "An electromagnetic sensor prototype to assist visually impaired and blind people in autonomous walking," *IEEE Sens. J.*, vol. 18, pp. 2568-2576, Mar. 2018.

[13] E. Cardillo, and A. Caddemi, "Insight on electronic travel aids for visually impaired people: a review on the electromagnetic technology," *Electronics*, vol. 8, pp. 1-12, Nov. 2019.

[14] S. M M Islam, N. Motoyama, S. Pacheco, V. M. Lubecke, "Non-contact vital signs monitoring for multiple subjects using a millimeter wave FMCW automotive radar," in *Proc. IMS 2020*, Los Angeles, CA, USA, 2020, pp. 1-4.

[15] D. Rodriguez and C. Li, "Sensitivity and distortion analysis of a 125-GHz interferometry radar for submicrometer motion sensing applications," *IEEE Trans. Microw. Theory Techn*, vol. 67, no. 12, pp. 5384-5395, Dec. 2019.

[16] S. Kim and C. Nguyen, "A displacement measurement technique using millimeter-wave interferometry," *IEEE Trans. Microw. Theory Techn*, vol. 51, no. 6, pp. 1724-1728, Jun. 2003.

[17] F. García-Rial et al., "Evaluation of standoff multistatic 3-D radar imaging at 300 GHz," *IEEE Trans. THz Sci. Technol.*, vol. 10, no. 1, pp. 58-67, Jan. 2020.

[18] Y. Nan, X. Huang and Y. J. Guo, "A millimeter-wave GCW-SAR based on deramp-on-receive and piecewise constant Doppler imaging," *IEEE Trans. Geosci. Remote Sens.*, vol. 58, no. 1, pp. 680-690, Jan. 2020.

[19] E. Cardillo, C. Li, and A. Caddemi, "Empowering blind people mobility: a millimeter-wave radar cane," *in proc. IEEE International Workshop on Metrology for Industry 4.0 and IoT*, Rome, Italy, 2020.

[20] A. Bhattacharya and R. Vaughan, "Deep learning radar design for breathing and fall detection," *IEEE Sens. J.*, vol. 20, no. 9, pp. 5072-5085, 1 May1, 2020, doi: 10.1109/JSEN.2020.2967100.

[21] E. Cardillo, and A. Caddemi, "Feasibility study to preserve the health of an Industry 4.0 worker: a radar system for monitoring the sitting-time," *in proc. IEEE International Workshop on Metrology for Industry 4.0 and IoT*, pp. 254-258, Naples, Italy, 2019.

[22] Y. Zhang et al., "Detection and identification of multiple stationary human targets via bio-radar based on the cross-correlation method," *Sensors*, Vol. 16, pp 1-12, Oct. 2016.

[23] Y. Yuan, C. Lu, A. Y. Chen, C. Tseng and C. M. Wu, "Multi-target concurrent vital sign and location detection using metamaterial-integrated self-injection-locked quadrature radar sensor," *IEEE Trans. Microw. Theory Techn*, vol. 67, no. 12, pp. 5429-5437, Dec. 2019.

[24] A. Prat, S. Blanch, A. Aguasca, J. Romeu and A. Broquetas, "Collimated beam FMCW radar for vital sign patient monitoring," *IEEE Trans. Antennas Propag.*, vol. 67, no. 8, pp. 5073-5080, Aug. 2019.

[25] G. Sacco, E. Piuzzi, E. Pittella, and S. Pisa, "An FMCW radar for localization and vital Signs measurement for different chest orientations," *Sensors*, vol. 20, no. 12, Jun. 2020.

[26] G. Wang, C. Gu, T. Inoue and C. Li, "A Hybrid FMCW-Interferometry Radar for Indoor Precise Positioning and Versatile Life Activity Monitoring," *IEEE Trans. Microw. Theory Techn*, vol. 62, no. 11, pp. 2812-2822, Nov. 2014.

[27] Z. Peng et al., "A portable FMCW interferometry radar with programmable low-IF architecture for localization, ISAR imaging, and vital sign tracking," *IEEE Trans. Microw. Theory Techn*, vol. 65, no. 4, pp. 1334-1344, Apr. 2017.

[28] F. Wang, T. Horng, K. Peng, J. Jau, J. Li, and C. Chen, "Detection of concealed individuals based on their vital signs by using a see-throughwall imaging system with a self-injection-locked radar," *IEEE Trans. Microw. Theory Techn.*, vol. 61, no. 1, pp. 696–704, Jan. 2013.

[29] A. Rahman, E. Yavari, A. Singh, V. M. Lubecke, and O.-B. Lubecke, "A low-IF tag-based motion compensation technique for mobile Doppler radar life signs monitoring," *IEEE Trans. Microw. Theory Techn.*, vol. 63, no. 10, pp. 3034–3041, Oct. 2015.

[30] F. Zhu, K. Wang, and K. Wu, "A fundamental-and-harmonic dualfrequency Doppler radar system for vital signs detection enabling radar movement self-cancellation," *IEEE Trans. Microw. Theory Techn.*, vol. 66, no. 11, pp. 5106–5118, Nov. 2018.

[31] J. Yan, Z. Peng, H. Hong, H. Chu, X. Zhu and C. Li, "Vital-SAR-imaging with a drone-based hybrid radar system," *IEEE Trans. Microw. Theory Techn*, vol. 66, no. 12, pp. 5852-5862, Dec. 2018.

[32] J. Yan, G. Zhang, H. Hong, H. Chu, C. Li and X. Zhu, "Phase-based human target 2-D identification with a mobile FMCW radar platform," *IEEE Trans. Microw. Theory Techn*, vol. 67, no. 12, pp. 5348-5359, Dec. 2019.

[33] D. Smardzija et al., "Applications of MIMO techniques to sensing of cardiopulmonary activity," in *Proc. IEEE/ACES International Conference on Wireless Communications and Applied Computational Electromagnetics*, Honolulu, HI, 2005, pp. 618-621.

[34] C. Will, P. Vaishnav, A. Chakraborty and A. Santra, "Human target detection, tracking, and classification using 24-GHz FMCW radar," *IEEE Sens. J.*, vol. 19, no. 17, pp. 7283-7299, Sept. 2019.

[35] H. Lee, B.-H. Kim, J.-K. Park, and J.-G. Yook, "A novel vital-sign sensing algorithm for multiple subjects based on 24-GHz FMCW Doppler radar," *Remote Sens.*, vol. 11 no. 10, May 2019.

[36] M. Alizadeh, G. Shaker, J. C. M. D. Almeida, P. P. Morita and S. Safavi-Naeini, "Remote monitoring of human vital signs using mm-wave FMCW radar," *IEEE Access*, vol. 7, pp. 54958-54968, Apr. 2019.

[37] E. Cardillo and A. Caddemi, "A novel approach for crosstalk minimization in FMCW radars," *Electron. Lett.*, vol. 53, pp. 1379-1381, Sept. 2017.

[38] Y. Xiong, Z. Peng, G. Xing, W. Zhang and G. Meng, "Accurate and robust displacement measurement for FMCW radar vibration monitoring," *IEEE Sens. J*, vol. 18, no. 3, pp. 1131-1139, Feb. 2018.

[39] A. Caddemi and E. Cardillo, "Optical control of gain amplifiers at microwave frequencies," in Proc. *Computing and Electromagnetics International Workshop (CEM17)*, Barcelona, Spain, 2017, pp. 51-52.

[40] C. Gu, J. Wang and J. Lien, "Deep neural network based body movement cancellation for Doppler radar vital sign detection," in Proc. *IEEE IWS 2019*, Guangzhou, China, 2019, pp. 1-3.

[41] W. G. Carrara, R. S. Goodman, and R. M. Majewski, Spotlight Synthetic Aperture Radar: Signal Processing Algorithms. Boston, MA, USA: Artech House, 1995.

[42] C. C. Chen, and H. C. Andrews, "Target-motion-induced radar imaging," *IEEE Trans. Aero. Elec. Sys.*, vol. 16, pp. 2-14, Jan. 1980.

[43] G. Wang, J.-M. Muñoz-Ferreras, C. Gu, C. Li, and R. Gómez-García, "Application of linear-frequency-modulated continuous-wave (LFMCW) radars for tracking of vital signs," *IEEE Trans. Microw. Theory Techn.*, vol. 62, pp. 1387-1399, Jun. 2014.

[44] J. Tu, T. Hwang and J. Lin, "Respiration rate measurement under 1-D body motion using single continuous-wave Doppler radar vital sign detection system," *IEEE Trans. Microw. Theory Techn*, vol. 64, no. 6, pp. 1937-1946, June 2016.

[45] Infineon BGT24MTR11 datasheet, Rev. 3.1, 2014-03-25.

[46] TRA_120_002_V0.8 Datasheet, Rev. 0.8, Silicon Radar GmbH, Frankfurt, Germany, 2018.

[47] C. Li, and J. Lin, "Signal processing," in *Microwave noncontact motion sensing and analysis*, Ed. New York, NY, USA: John Wiley & Sons, Inc, 2013, pp. 141–142.

Emanuele Cardillo (M'15) received his MSc degree in Electronic Engineering from the University of Messina, Italy, and Ph.D degree from the University Mediterranea of Reggio Calabria, Italy, in 2013 and 2018, respectively. He is currently postdoctoral researcher at the University of Messina. His current research interests are focused on the microwave electronics field, mainly on short-range radar systems and interferometry techniques, design of active and passive planar hybrid microwave integrated circuits (HMIC), linear and noise modeling of microwave field-effect transistors, linear and noise microwave measurements and realization of HMIC circuits and systems. He served as a member of the organizing committee of the International Workshop on Integrated Nonlinear Microwave and Millimetre-wave circuits (INMMIC 2015). He serves as a member of the scientific committee of the International Conference on Microelectronic, Devices and Technologies (MicDAT). He was the recipient of the "IEEE Sensors Journal Best Student Paper Award" (2017/2018) and of the "IEEE Microwave Theory and Techniques (MTT-S) award" (2018).

Alina Caddemi (M'13) received the degree in Electronic Engineering (honors) and the Ph.D. degree from the University of Palermo, Italy, in 1982 and in 1987, respectively. In 1984, she joined the Electrical engineering Dept. at the University of Utah, USA, and in 1985 the Electrical and Computer Engineering Dept. at the University of Colorado, Boulder, USA, as a visiting researcher in the field of microwave bioelectromagnetics. From 1990 to 1998, she was with the Department of Electrical Engineering, University of Palermo, as an assistant professor. In 1998 she joined the University of Messina, Italy, where she is currently Full professor of Electronics and the supervisor of the Microwave Electronics (ELEMIC) Lab. Her current research interests are in the field of temperature-dependent linear and noise characterization techniques for solid-state devices, cryogenic measurements and modeling of field-effect transistors, noise modeling of bipolar and field-effect transistors, neural network modeling of field-effect transistors, design and realization of hybrid low-noise components and circuits, compact radar systems for short-range applications. She has authored or co-authored more than 250 papers on international scientific journals and conference proceedings. She has been the partner team leader for several national and international projects. She has served as an Associate Editor of the International Journal of Numerical Modelling: Electronic Networks, Devices and Fields and in the Editorial Board of Microwave Review, a publication of the national Society for Microwave Technique, Technologies and Systems for Serbia and Montenegro IEEE MTT-S Chapter. She is presently an Editorial Board Member of Electronics MDPI.